

Adaptive orthogonalization of opponent-color signals

Qasim Zaidi, Arthur G. Shapiro

Department of Psychology, 406 Schermerhorn Hall, Columbia University, New York, NY 10027, USA

Received: 12 January 1993/Accepted in revised form: 21 April 1993

Abstract. This paper concerns the processing of the outputs of the two opponent-color mechanisms in the human visual system. We present experimental evidence that opponent-color signals interact after joint modulation even though they are essentially independent under neutral steady adaptation and after exclusive modulation of each mechanism. In addition, prolonged modulation linearizes the response function of each mechanism. The changes in interaction serve to orthogonalize opponent signals with respect to the adapting modulation, and the changes in response functions serve to equalize the relative frequencies of different levels of response to the adapting modulation. Adaptive orthogonalization reduces sensitivity to the adapting color direction, improves sensitivity to the orthogonal direction, and predicts shifts in color appearance. Response equalization enhances effective contrast and explains the difference between the effects of adaptation to uniform versus temporally or spatially modulated stimuli.

1 Introduction

For over a century, human color vision has been explained in terms of the responses of three independent classes of cone photoreceptors and the linear combination of cone outputs into three independent mechanisms, two opponent-color and one luminance. During this period, quantitative estimates of the absorption spectra of the cones and the second-stage combination rules were progressively refined to the point of general agreement. (For historical and mathematical background see Zaidi 1992.) Little thought was given to later stages of color processing, because it seemed that the results of most color experiments could be adequately explained in terms of these mechanisms. However, the systematic nature of deviations was difficult to judge because stimuli were generally specified either in terms of spectral composition or in terms of location in the CIE chromaticity

diagram rather than on a mechanistic basis [Judd (1932) and Le Grand (1949) being exceptions]. Recently, some experiments on chromatic discrimination, adaptation and induction directly examined the effects of stimulating opponent mechanisms exclusively and jointly (Table 1). The results of these experiments deviate systematically from predictions based on independent opponent mechanisms and provide clues to the identity of post-opponent processes. At a qualitative level, Krauskopf et al. (1986a, b) suggested that such results can be explained in terms of the responses of multiple (more than two) classes of "higher-order color mechanisms" which process the outputs of the two independent opponent classes. We present an alternative quantitative model that consists of just the two classes of opponent mechanisms but allows for an adaptable degree of interaction between their signals. Each state of adaptation is defined by a constant magnitude of mutual inhibition or excitation (possibly zero) between the two signals. This magnitude can change as a function of the history of stimulation.

To demonstrate that the magnitude of interaction changes adaptively, we present an elaborated version of the chromatic adaptation experiment that provided the initial impetus for higher-order color mechanisms (Krauskopf et al. 1986a). In the elaborated version, theoretically specified stimuli were used to measure the response (input-output) functions of the two opponent mechanisms and the degree of interaction between them, first during steady neutral adaptation, and then following prolonged viewing of a light that maintained the same average color while its chromaticity was slowly modulated. This type of modulation is believed to modify the responses of opponent mechanisms without affecting cone sensitivities (Krauskopf et al. 1982). We used adapting chromatic directions that stimulated the mechanisms either exclusively or jointly. Comparison of the pre- and post-adaptation interaction measurements supported the theory that joint stimulation of opponent mechanisms changes the degree of interaction between their signals (Zaidi and Shapiro 1992a, b; Shapiro and Zaidi 1992a). This process is similar to the adaptive orthogonalization (Kohonen and Oja 1976; Kohonen 1984) and decorrelation (Barlow and Földiák 1989; Barlow 1990) processes that have been postulated in other neural domains.

Table 1. Chronological list of experimental results requiring post-opponent color processes

Experiment	Reference
1. Adaptation to prolonged temporal modulation of color (threshold elevations)	Krauskopf et al. (1986a)
2. Transient change of chromatic adaptation	Krauskopf et al. (1986a)
3. Detection and discrimination of step color changes	Krauskopf et al. (1986a)
4. Induced simultaneous contrast	Krauskopf et al. (1986b)
5. Color discrimination	Boynton et al. (1986)
6. Tilt after-effect	Flanagan et al. (1990)
7. Adaptation to prolonged temporal modulation of color (asymmetric color matches)	Webster and Mollon (1991)
8. Masking by chromatic and luminance noise	Gegenfurtner and Kiper (1992)
9. Discrimination between suprathreshold color changes	Zaidi and Halevy (1991, 1993)

After adaptation to a sinusoidally modulated light the differential sensitivity of each opponent mechanism was significantly more uniform over the response range than during adaptation to a steady light of the same average color, indicating that the shape of each response function depends on the distribution of inputs in the adapting stimulus rather than on just the average input. In particular the adaptive changes could not be explained by any reasonable notion of "fatigue". The functional model we propose for this type of adaptation is similar to the histogram transformation techniques used in digital image enhancement (Rosenfeld and Kak 1982; Gonzalez and Wintz 1987).

2 Post-opponent chromatic mechanisms

We assume that cone spectral sensitivities (L, M, S) correspond to the Smith and Pokorny (1975) fundamentals, and the second-stage mechanisms (RG, YV, V_λ) to those defined by the Krauskopf et al. (1982) cardinal axes. (For a detailed justification, see Zaidi 1992.) In Fig. 1 we present a model of the chromatic mechanisms that follow the opponent combination of cone signals. The first three stages constitute the mechanistic portion of the model. The first stage consists of two opponent signals (rg, yv) that are linear combinations of cone outputs (l, m, s):

$$rg \propto l - 2m \quad (1a)$$

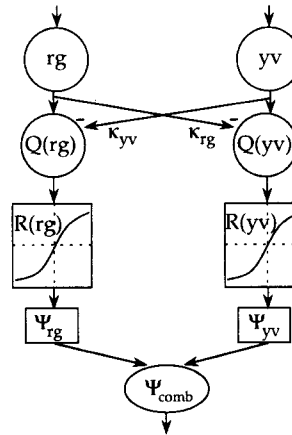
$$yv \propto s - 0.023(l + m) \quad (1b)$$

At the second stage a fraction κ_i of each signal is subtracted from the other (throughout this paper, the subscripts "i" and "j" refer to "rg" or "yv"):

$$Q_{rg} = rg - \kappa_{yv} yv \quad (2a)$$

$$Q_{yv} = yv - \kappa_{rg} rg \quad (2b)$$

Signals from the two mechanisms do not interact if κ_{yv} and κ_{rg} are equal to zero. The third stage assumes that in any state of adaptation each opponent mechanism has a limited response range described by logarithmic compressive functions with parameters α and β on each side

**Fig. 1.** Model for the post-opponent processing of chromatic signals

of the adaptation level ($Q = 0$):

$$R_i = \frac{1}{\beta_i^+} \log(\alpha_i + \beta_i^+ Q_i) - \frac{1}{\beta_i^+} \log(\alpha_i) \quad \text{if } Q_i \geq 0 \quad (3a)$$

$$R_i = \frac{1}{\beta_i^-} \log(\alpha_i + \beta_i^- Q_i) - \frac{1}{\beta_i^-} \log(\alpha_i) \quad \text{if } Q_i < 0 \quad (3b)$$

For each mechanism there is one value of α_i , but possibly different magnitudes of $\beta_i^+ > 0$ and $\beta_i^- < 0$ for positive and negative values of Q_i , respectively. The complete response function is thus S-shaped and passes smoothly through $(0, 0)$ with different amounts of compression in the positive and negative limbs. This form of the response function was chosen to set the differential response dR/dQ equal to $1/(\alpha + \beta Q)$ on each side of $Q = 0$. The differential response is inversely proportional to βQ , therefore greatest at the adaptation point. In those conditions where $\beta = 0$, the differential response is equal to a constant $(1/\alpha)$ for the whole range of inputs, and $R = Q/\alpha$.

The static nonlinearity in (3) enables the model to account for chromatic discrimination at the adaptation point and other loci during a state of constant adaptation. Fitting the model to chromatic discrimination thresholds, i.e. estimating values of α , β , and κ , requires an explicit decision rule. The last two stages depict one probabilistic decision rule and will be discussed in Sect. 6 after the description of the experimental procedure.

3 Specification of color stimuli

We specified our stimuli in terms of their effect on the two opponent mechanisms. The entire range of lights used in this study is specified as a quadrilateral in Fig. 2 on a plane formed by two cardinal axes, RG and YV . The axes are specified in (L, M, S) cone excitations (MacLeod and Boynton 1979). The center of the plane (W) is an achromatic white. Lights along the vertical (YV) axis vary only in S -cone excitations. Along the horizontal (RG) axis, S -cone excitation is constant, whereas L and M cone excitations change in equal and opposite fashion. These axes are taken as orthogonal because transitions between lights along each axis stimulate only the corresponding opponent mechanism (1a, 1b). Krauskopf et al. (1982) showed that adaptation to prolonged temporal modulation along either cardinal axis did not affect thresholds along the orthogonal axis. In addition, within the equiluminant plane, macaque lateral geniculate nucleus (LGN) parvoneurons in the $\pm(L - M)$ class are stimulated exclusively by modulations along the RG direction, and neurons in the $\pm[S - (L + M)]$ class by modulations along YV (Derrington et al. 1984). The units along the axes are multiples of the amplitudes of thresholds at W measured during steady adaptation to W , and will be used throughout the paper. These units also specify lights in terms of angular direction around W .

The lights in Fig. 2 differed in chromaticity but were all at a luminance of 50 cd/m^2 , thus excluding the luminance mechanism from responding to any transitions between these lights. The two opponent mechanisms were stimulated exclusively by modulating chromaticities along one of the two cardinal directions, and stimulated jointly to a specified degree by chromaticities along the appropriate intermediate line.

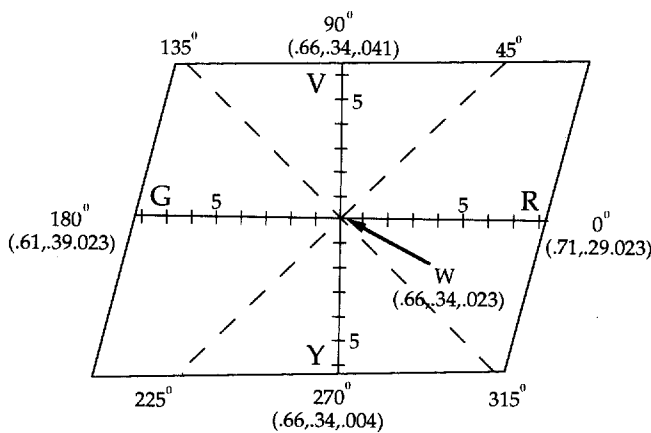


Fig. 2. The quadrilateral represents the range of equiluminant lights (50 cd/m^2) used in this study. The center and the ends of the axes are specified in (L, M, S) cone excitations. W , the center of the plane is an achromatic white. Lights along the vertical (YV) axis vary only in S -cone excitations. Along the horizontal (RG) axis, S -cone excitation is constant whereas L - and M -cone excitations change in equal and opposite fashion. Units along axes are multiples of the threshold amplitudes at W . Lights are also specified in terms of angular direction from W .

4 Equipment

Stimuli were displayed on the screen of a Tektronix 690SR color monitor refreshed at the rate of 120 interlaced frames/second. Images were generated using an Adage 3000 raster-based frame-buffer generator. 1024 output levels were specifiable for each gun. Up to 256 colors could be displayed on the screen in any frame. The color of an image was modulated sinusoidally in time by cycling through a pre-computed color array. Up to 240 colors could be changed during the fly-back interval in a screen refresh. The 512×480 pixel display subtended an angle of $10.67^\circ \times 10^\circ$ at the observer's eye. Details of the calibration and color specification can be found in Zaidi and Halevy (1993) and Sachtler and Zaidi (1992). All stimulus presentation and data collection was done under automatic computer control.

5 Experimental procedure

We estimated the parameters of the response functions and the magnitude of interaction from sets of chromatic discrimination thresholds. For a set of pre-determined points (F) on the color plane, the procedure outlined in Fig. 3 was used to measure the distance P along a pre-determined color line at which the observer could discriminate between the two colors $F + 0.5P$ and $F - 0.5P$ with a probability of 0.71. Thresholds were measured both during steady adaptation to W , the pre-adaptation condition, and after the color of the field had been modulated sinusoidally (1 Hz) symmetrically around W to the ends of the plane along one of the $0-180^\circ$, $45-225^\circ$, $90-270^\circ$, or $135-315^\circ$ lines in Fig. 2, the post-adaptation condition. In the pre-adaptation condition, the observer initially adapted to a steady field metameric to W for 120 s. The steady W field was on for an additional 0.6 s to make the pre- and post-adaptation conditions similar. For a period of 0.25 s the field flashed to the color F . During the first 0.025 s of the flash, a probe was presented as two halves of a disk, one half at $F + 0.5P$

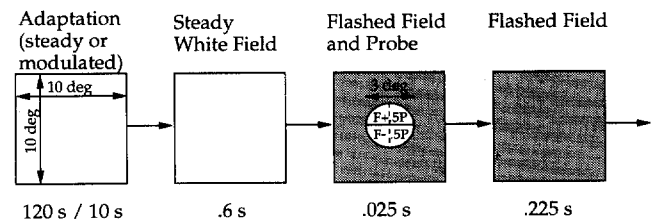


Fig. 3. Experimental procedure. The observer initially adapted to a steady, $10^\circ \times 10^\circ$ field metameric to W (120 s). For a period of 0.25 s the field flashed to a pre-determined color (F). During the first 0.025 s of the flash, a probe was presented as two halves of a disk (one at $F + 0.5P$, the other at $F - 0.5P$). The observer indicated whether the division of the disk was horizontal or vertical. After each trial the observer re-adapted to W (10 s). After pre-adaptation thresholds were measured, the observer adapted to sinusoidal temporal modulation of the color of the 10° square field (120 s). Thresholds for the same combination of F and P were remeasured. After each trial there was 10 s of re-adaptation.

and the other at $F - 0.5P$. The division of the disk was randomly presented as horizontal or vertical, and the observer had to make a forced choice as to the orientation. After each trial the observer re-adapted to W for 10 s. A double random staircase was used to vary P , the probe amplitude along the pre-determined color line. Threshold was calculated as the mean of 12 transitions. In the post-adaptation conditions, the observer adapted for 120 s to temporal modulation of the color of the 10° field along one color line. Thresholds at the same set of points F and the same color directions of P as the pre-adaptation condition were remeasured by the same procedure. After each trial there was 10 s of re-adaptation to the modulation. A steady W field was presented for 0.6 s after each modulation interval to let any transitory effects die out and to restore the adaptation level of the cone photoreceptors to W . The probe was presented for a period brief enough to not significantly affect the state of adaptation, while allowing for thresholds to be measured for a range of combinations of F and P (Zaidi et al. 1992). We were thus able to measure discrimination thresholds at the adaptation point and other loci in the same state of adaptation. As will be shown below, we estimated the response and interaction parameters of the model by using flashes (F) along one cardinal axis and probes (P) in the parallel or orthogonal direction.

Complete sets of data were collected for the second author (A.S.) and a naive observer (K.B.). Both observers had normal color vision and acuity.

6 Decision rule

The last two stages of the model in Fig. 1 depict the decision rule used to fit the model to the discrimination thresholds. At the fourth stage, for every stimulus combination of F and P , the model generates values for ψ_i 's, the independent probabilities of discriminating between $F + 0.5P$ and $F - 0.5P$ by each mechanism. For each F_i this probability was assumed to be proportional to $R(F_i + 0.5P_i) - R(F_i - 0.5P_i)$, thus generating a psychometric function that monotonically increases with probe amplitude. For analytical convenience, this probability was approximated by the differential response of the mechanism (slope of the response function in Eq. 3) at the level corresponding to the input F_i , multiplied by the input to the response function from the probe amplitude P_i :

$$\psi_i = 0.71 \left| \frac{Q(P_i)}{dQ_{Q=Q(F_i)}} \frac{dR}{dQ} \right| = 0.71 \left| \frac{Q(P_i)}{\alpha_i + \beta_i Q(F_i)} \right| \quad (4)$$

The probability of discrimination by the observer was calculated as the joint probability of discrimination by either one or both of the mechanisms:

$$\psi_{comb} = 1 - (1 - \psi_{rg})(1 - \psi_{yv}) = \psi_{rg} + \psi_{yv} - \psi_{rg}\psi_{yv} \quad (5)$$

Given a set of parameters and the projected flash amplitudes (F_{rg}, F_{yv}), the model predicted threshold to be equal to the amplitude in the probe direction (P_{rg}, P_{yv}) for which the combined probability equalled a criterion level of 0.71.

7 Pre-adaptation results

In Fig. 4, the open circles show the amplitude of pre-adaptation probe thresholds (P_i) along one of the cardinal axes, as functions of the flash amplitude (F_i), defined as the number of units along a cardinal axis between the flashed mid-point of the two halves of the probe disk and the adaptation point W . The dashed lines show the best fits of the model to the pre-adaptation data. Each panel shows results for distinct flash and probe direction combinations. The units along the abscissa and the ordinate are equal to the units on the corresponding cardinal axes in Fig. 2. The inset in the top right corner of each panel depicts a typical combination of F and P on an outlined replica of the color plane from Fig. 2.

In Fig. 4A, the inset indicates that flash colors (dot) were located on the RG axis, and the two halves of the probe (arrowheads) differed along the same axis. The open circles show that threshold amplitudes were smallest at the steady adaptation point ($F_{rg} = 0$) and increased on both sides with increasing flash amplitude. If there is no interaction between the mechanisms, then the transition from W to flashes and probes on the RG axis does not stimulate the YV mechanism, so that in the model $Q(F_{yv}) = Q(P_{yv}) = 0$, $Q(F_{rg}) = F_{rg}$ and $Q(P_{rg}) = P_{rg}$. Consequently, (4) and (5) predict that on each side of $F_{rg} = 0$ the threshold probe amplitude should be a linear function of the flash amplitude:

$$P_{rg} = \alpha_{rg} + \beta_{rg} F_{rg} \quad (6a)$$

In the condition in Fig. 4B, the inset shows that flashes were metameric to colors on the YV axis and the probe halves differed along the same axis. The pattern of results is similar to that for the RG axis. Under similar assumptions of zero interaction as in (6a), the model predicts:

$$P_{yv} = \alpha_{yv} + \beta_{yv} F_{yv} \quad (6b)$$

The reasonably good fits of the dashed lines to the open circles in Fig. 4A, B indicate that the logarithmic response functions in the model provide a suitable substrate for the probe thresholds. In addition, on each side of the adaptation point, the intercept and slope of the best-fitting regression line provide estimates of α_i and β_i , respectively.

The magnitude of interaction was estimated from the differential response of each mechanism at increasing activation levels of the other mechanism. As the insets in Fig. 4C, D indicate, probe thresholds parallel to each cardinal axis were measured at different flash points along the orthogonal axis. In Fig. 4C, D some of the open circles are obscured by the filled symbols, and the dashed lines are obscured by the solid lines. If κ_i 's are small, the model predicts that probe thresholds parallel to one axis should increase approximately linearly with the amplitude of flashes on the orthogonal axis, such that for Fig. 4C:

$$\text{magnitude of the slope} = \kappa_{rg} \beta_{yv} \quad (7a)$$

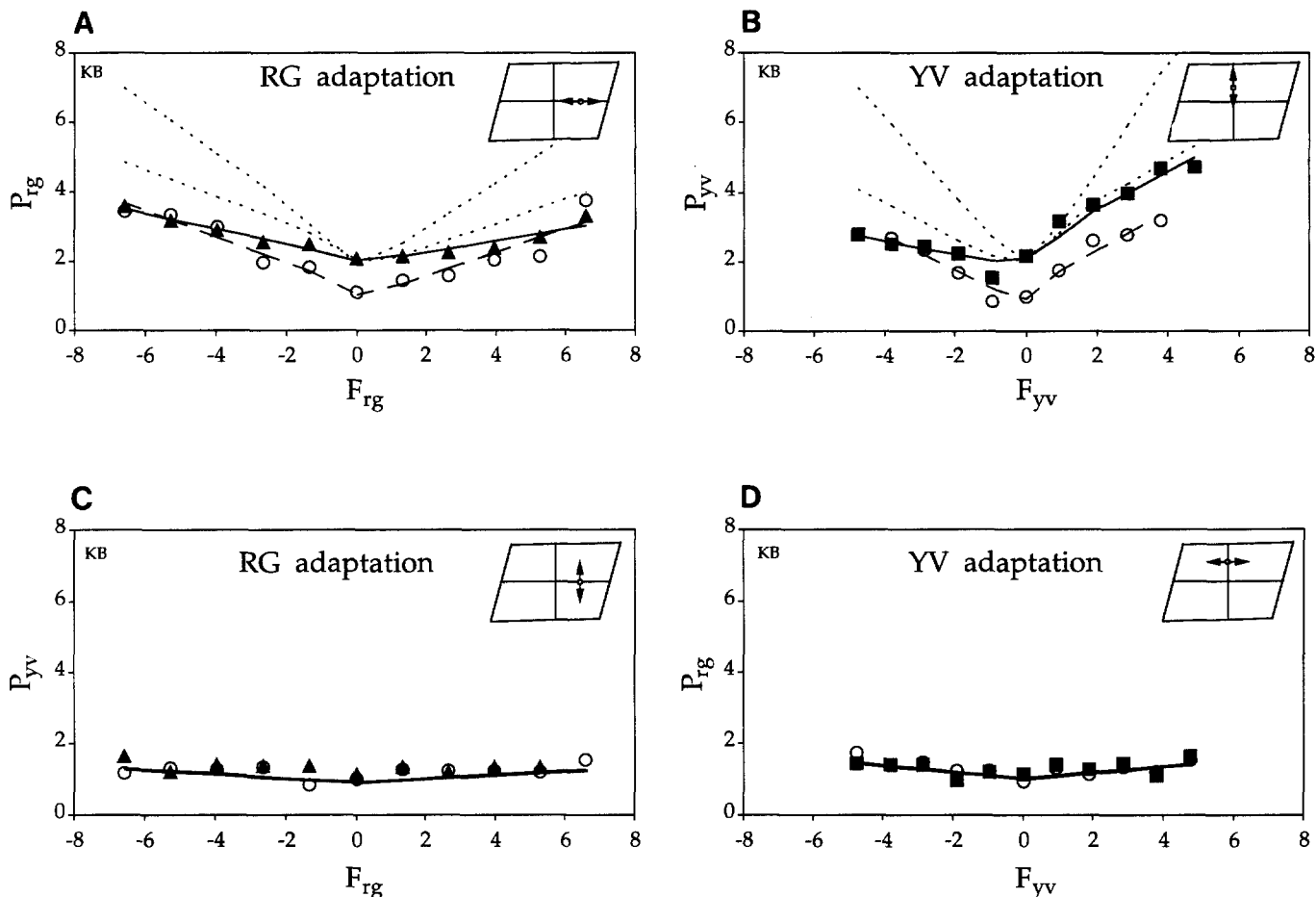


Fig. 4A–D. Comparison of pre-adaptation thresholds (\circ) with post-RG adaptation (\blacktriangle) and post-YV adaptation (\blacksquare). Dashed and solid curves are the best fits of the pre- and post-adaptation models, respectively. For the pre- and each post-adaptation condition, all parameters of the model were simultaneously optimized to the four panels using a Nelder-Meade simplex algorithm. The inset in each panel refers to the

color plane (Fig. 2): the dot shows the location of a typical flash and the arrows indicate the color direction in which the two halves of the probe were varied. Probe amplitudes (P_{rg} or P_{yv}) are plotted against flash amplitudes (F_{rg} or F_{yv}) in threshold units of the cardinal axes. Standard errors were 10–20% of the mean value. Data are presented for one color-normal observer, K.B.

and for Fig. 4D:

$$\text{magnitude of the slope} = \kappa_{yv} \beta_{rg} \quad (7b)$$

If there were no interaction between the mechanisms, the threshold curves would have zero slopes. However, the threshold curves are shallow but not perfectly flat; therefore, the estimated κ_i 's were small but not zero, indicating minimal interaction between the mechanisms under steady adaptation to W . Since the magnitudes of the slopes are small, estimates of κ_i 's by this method can vary over a small range.

Because the analytic expressions in (6a, b) and (7a, b) were derived on the basis of restrictive assumptions, we used the estimates of the parameters based on these equations as approximations. These approximations were used as starting values for a Nelder-Meade simplex algorithm (Press et al. 1988) which varied the values of all parameters of the model to find the best simultaneous fit to the four sets of discrimination thresholds. The predicted threshold curves in the figures in this paper are

based on the Nelder-Meade estimates. For the preadaptation data, the Nelder-Meade estimates were close to those derived from the analytic expressions.

8 Processes of adaptation to modulated stimuli

In terms of the model, we assume that adaptation to sinusoidal modulation of colors around a constant dc level can modify both the response of each mechanism (Fig. 5A) and the magnitude of interaction (Fig. 5B). The three models in Fig. 5A make distinct predictions for thresholds measured at flashed loci on the same cardinal axis as the probe direction:

Fig. 5A top. If the effect of adaptation can be represented as a multiplicative attenuation of the gain of the signal that is input to the nonlinear response function, i.e. $Q_{post} = Q_{pre}/\mu$, then from (4) the model predicts post-adaptation threshold curves that have intercepts elevated by the factor μ , but slopes identical to pre-adaptation thresholds. If α_i and β_i are the pre-adaptation response

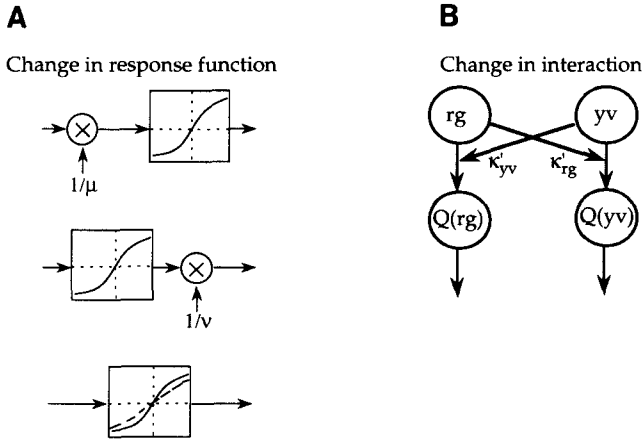


Fig. 5. Models: **A** Three possible effects of adaptation on the response function; **B** change in interaction parameters as a result of adaptation

parameters, then after adaptation:

$$P_i = \mu\alpha_i + \beta_i F_i \quad (8a)$$

Fig. 5A middle. If the effect can be represented as a multiplicative attenuation of the gain of the output signal of the nonlinear response function, i.e. $R_{post} = R_{pre}/\nu$ so that the derivative $dR/dQ_{post} = dR/\nu dQ_{pre}$, then from (4), the model predicts elevations of both the intercept and slope of the post-adaptation threshold curves by the same factor ν .

$$P_i = \nu\alpha_i + \nu\beta_i F_i \quad (8b)$$

Fig. 5A bottom. If the form of the nonlinearity is itself adaptive, then adaptation could lead to independent changes in α_i and β_i of the logarithmic form of the response function. In this case threshold curves should remain linear, but with independent changes in intercept and slope from the pre-adaptation condition:

$$P_i = \alpha_{i(post)} + \beta_{i(post)} F_i \quad (8c)$$

Fig. 5B. The effect of a change in the interaction parameters can be less obvious on the graphs. As (7a, b) indicates, if β_i 's do not change, then an increase in $\kappa_j (j \neq i)$ predicts an increase in the slope of the probe thresholds measured parallel to one axis against the amplitude of flashes on the orthogonal axis. However, if β_i 's are affected by the adaptation procedure, then even no change in slope can indicate a change in the magnitude of interaction between the two mechanisms.

9 Post-adaptation results (RG and YV)

Figure 4 also shows post-adaptation thresholds for the same combinations of F and P measured after adaptation to modulation along the RG (triangles) or YV (squares) axes. Compared to the pre-adaptation results, after RG adaptation (Fig. 4A), thresholds for P_{rg} are maximally elevated at $F_{rg} = 0$ and have shallower slopes.

The multiplicative gain control factors μ and ν of the adaptation models were estimated from the ratio of post-adaptation to pre-adaptation intercepts [(8a, b) vs (6a, b)]. The dotted lines parallel to the pre-adaptation curves are the prediction from (8a), the dotted lines with the steeper slopes from (8b). Neither multiplicative gain change model fits the data. It is obvious that no combination of the two multiplicative models will fit the data either. The solid lines are predictions from (8c) and provide a good fit. The effect of adaptation to color modulation was to increase the magnitude of α_{rg} and decrease the magnitude of β_{rg} , thus attenuating the differential response at the dc level but expanding the approximately linear range of response. Similarly, after YV adaptation (Fig. 4B) the change in YV thresholds as a function of YV flashes was not consistent with either multiplicative model (dotted lines), but could be explained by changing both α_{yv} and β_{yv} (solid lines). Previous studies of adaptation to color modulation measured thresholds only at W , i.e. intercepts, and therefore could not distinguish between these three possibilities.

Figure 4C, D shows the effect of RG and YV adaptation, respectively, on the interaction between the mechanisms. The post- and pre-adaptation points overlap, indicating no significant change in κ 's. The post-adaptation β 's are smaller, therefore for slopes equal to pre-adaptation slopes, the post-adaptation κ 's are slightly greater (7a, b).

Consistent with minimal interaction, RG adaptation did not appreciably affect the magnitude of the P_{yv} thresholds measured at F_{yv} loci, and YV adaptation did not affect P_{rg} thresholds measured at F_{rg} loci. Prolonged stimulation along each cardinal axis, therefore, mainly modified the response parameters of the corresponding mechanism.

10 Post-adaptation results (45–255° and 135–315°)

Temporal modulation along the 45–225° color line stimulates the RG and YV mechanisms jointly, such that in the units of Fig. 2, $rg(t) = yv(t)$ for all times t during the modulation. For modulation along 135–315°, $rg(t) = -yv(t)$. Post-adaptation measurements of (F_{rg}, P_{rg}) and (F_{yv}, P_{yv}) combinations showed that joint stimulation affected both response functions in a manner similar to exclusive stimulation, but each effect was less pronounced than exclusive stimulation of that mechanism. The interesting results are the effects on interactions shown in Fig. 6A–D. Figure 6A–D shows pre-adaptation thresholds (circles, same data as Fig. 4C, D) and thresholds measured after adaptation to modulation along 45–215° (squares) and 135–315° (triangles). The increase in P_i threshold at $F_j = 0$ reflects the change in the response function of the “ i ” mechanism. The pre- and post-adaptation slopes are different, indicating a significant increase in interaction between opponent mechanisms as a result of joint stimulation. These sets of thresholds can provide information about the magnitude but not the sign of the interaction parameters.

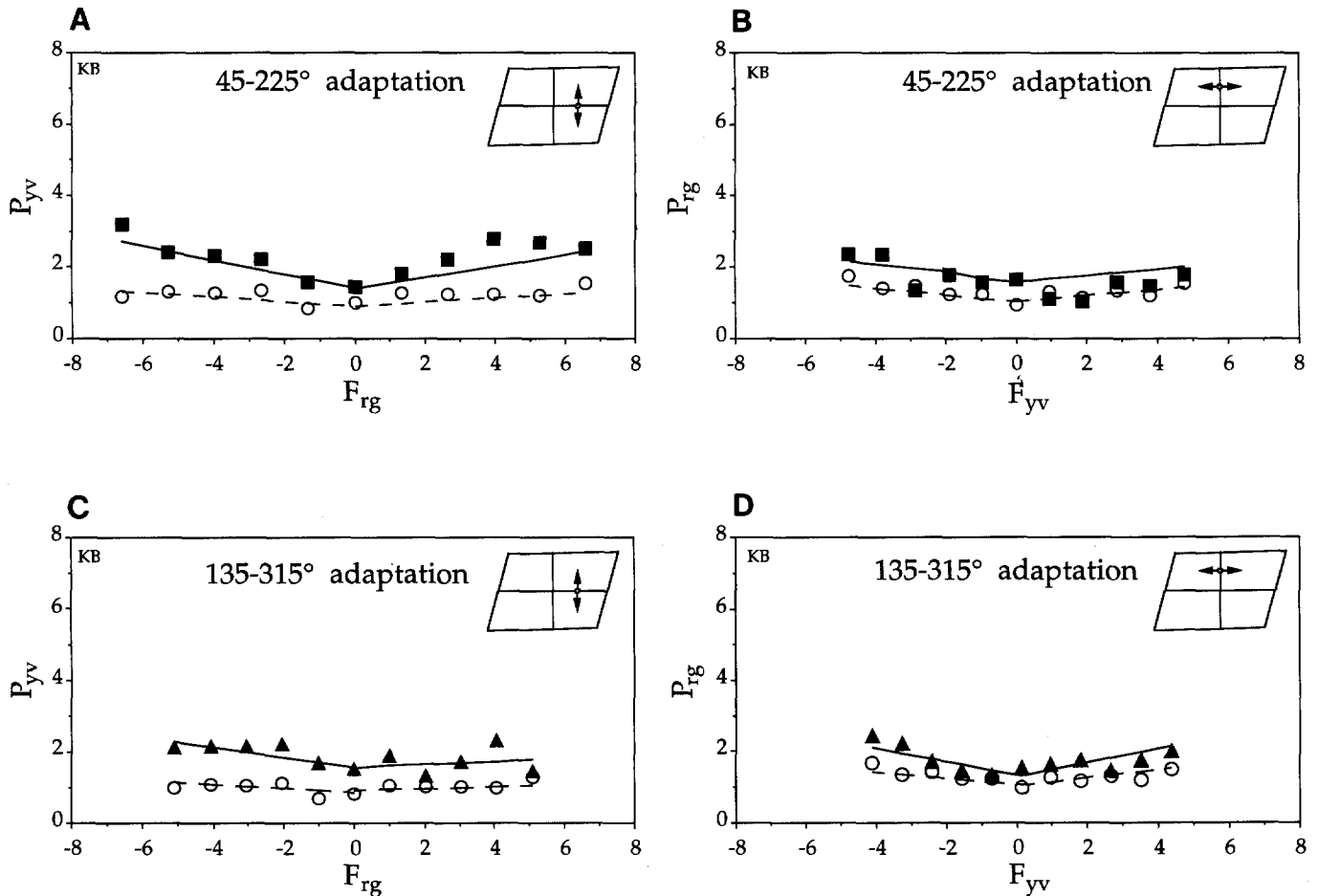


Fig. 6A-D. Comparison of pre-adaptation thresholds (\circ) to post-45-225° adaptation (\blacksquare) and post-135-315° adaptation (\blacktriangle). Other conventions similar to Fig. 4

11 Combination of opponent signals in intermediate color directions

Since transitions from W to points on intermediate color lines stimulate both opponent mechanisms simultaneously, magnitudes of probe thresholds in intermediate directions can also be used to test models of the combination of opponent signals. In this section we compare pre- and post-adaptation thresholds measured at W along the 0, 22.5, 45, 67.5, 90, 112.5, 135, and 157.5° directions. This portion of the study is a modified version of the Krauskopf et al. (1982, 1986a) adaptation experiment. The differences (Fig. 3) are that we used a forced-choice procedure, different spatial and temporal conditions, and probes that varied symmetrically on both sides of W . The results, however, were qualitatively similar.

The insets in the top-right corners of Fig. 7A-D indicate that all four graphs present probe thresholds measured at W in cardinal and intermediate directions. The abscissae represent the projection of the threshold probe amplitude on the RG axis and the ordinates the projection on the YV axis. The units on the axes correspond to the units in Fig. 2. The open circles in all four panels represent the same set of mean pre-adaptation

thresholds. The angle subtended by the line joining each open circle to the origin indicates the color direction of the probe, and the radial distance from the origin is equal to the threshold amplitude. The bars through the means represent plus and minus one standard deviation in the probe direction. Collectively, the pre-adaptation data have a circular form. The dotted line is the best fit of the model constrained to have zero interaction. The reasonably good fit corroborates the earlier result that under neutral steady adaptation the two opponent mechanisms do not interact appreciably, and demonstrates that thresholds in intermediate directions can be predicted by the probability summation decision rule.

The filled circles in Fig. 7A-D show probe thresholds in intermediate directions measured after adaptation to modulation along 0-180°, 90-270°, 45-225°, and 135-315°, respectively (label on top of each panel). In each of the four panels, the solid line indicates the best fit of the model to the data in the panel, and the dashed line indicates the best fit when the model was constrained to have zero interaction between the mechanisms.

Figure 7A shows that adaptation to modulation along the RG direction elevated threshold maximally along the RG axis, but did not significantly affect

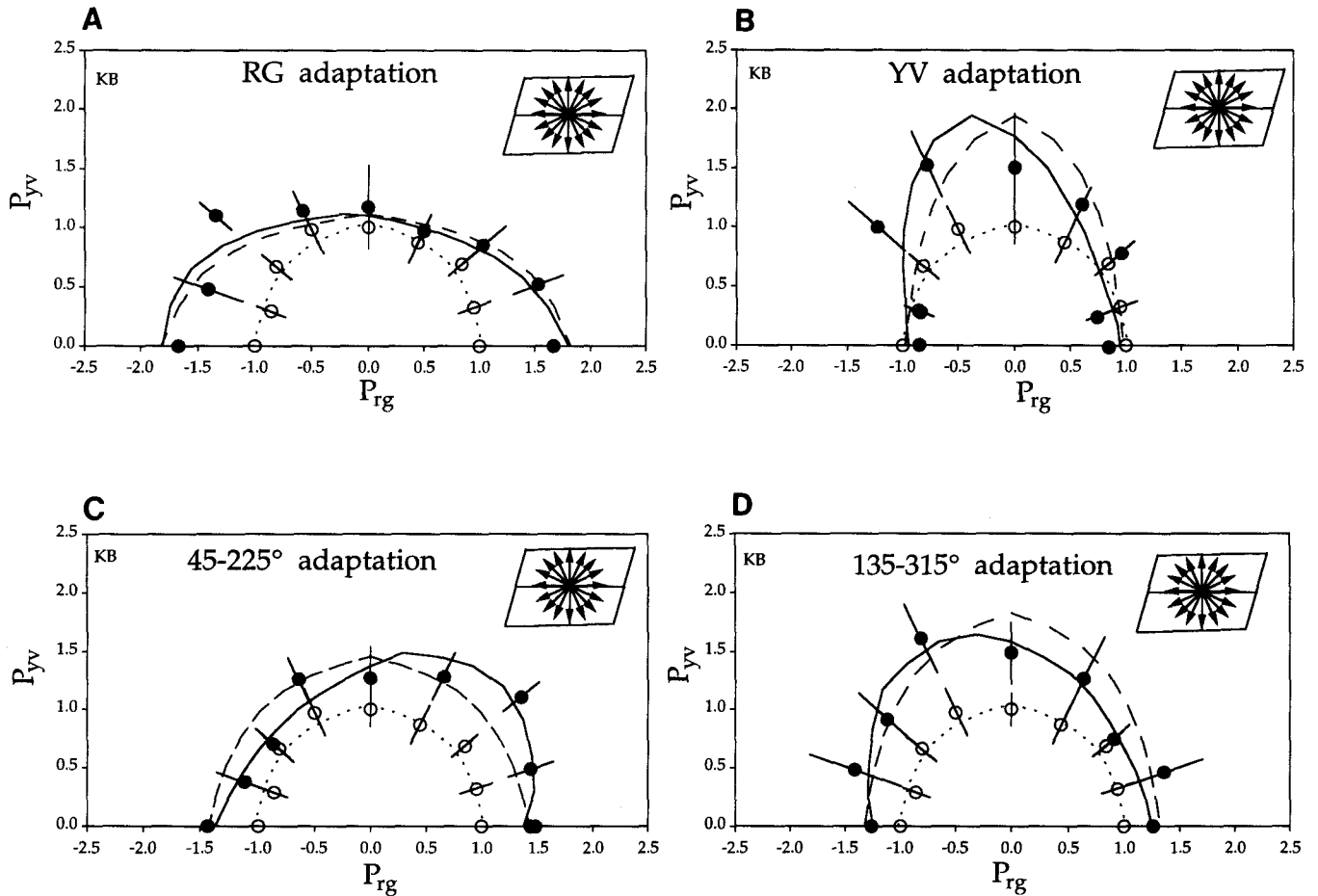


Fig. 7A–D. Comparison of pre- and post-adaptation probe thresholds measured at W along the 0, 22.5, 45, 67.5, 90, 112.5, 135, and 157.5° directions (insets in the top right corners). The ordinate represents the projection of the threshold probe amplitude on the RG axis and the abscissa the projection on the YV axis, both in the units in Fig. 2. *Open circles* represent mean pre-adaptation thresholds, and *bars* through the means represent plus and minus one standard deviation and are plotted

in the probe direction. The dotted line is the best fit of the model constrained to have zero interaction. The *filled circles* show probe thresholds measured after adaptation to **A** RG , **B** YV , **C** 45–225°, and **D** 135–315°. The *solid line* is the best fit of the model to the data in the panel, and the *dashed line* is the best fit when the model was constrained to have zero interactions

threshold along the YV axis. In the model this corresponds to changes in the RG response function combined with no change in the YV response function. The solid and dashed curves are similar and both provide reasonably good fits to the data, corroborating the earlier analysis that RG adaptation did not significantly affect the interaction between the two mechanisms. Figure 7B shows that adaptation to modulations along the YV direction did not significantly elevate thresholds along the RG axis, and had the maximum effect in the YV and 112.5° directions. The dashed curve shows the best fit of the model when only the response parameters of the YV and RG mechanisms were allowed to vary. The solid line shows the best fit when response and interaction parameters were all allowed to vary. Whereas the solid curve provides a better fit to the data, the dashed curve cannot be rejected.

Adaptation to modulations along the 45–225° and 135–315° directions (Fig. 7C, D) had the effect of elevating thresholds along both cardinal axes, indicating

changes in both RG and YV response functions. In both cases, the maximum increase in threshold was at or near the color direction of the adapting modulation and there was no significant elevation in the orthogonal direction. In the 45–225° adaptation panel (Fig. 7C), the fit of the model with positive κ_i 's (solid curve) is better than the fit of the model with zero interaction (dashed curve), especially in the 45° and 135° probe directions. In the 135–315° adaptation panel (Fig. 7D), the best fit with negative κ_i 's (solid curve) is better than the zero interaction fit (dashed curve), especially towards the 45° probe direction. In both Fig. 7C and Fig. 7D, the solid lines correctly predict no significant threshold elevation in the direction orthogonal to the adaptation, whereas the dashed lines incorrectly predict an elevation. This difference highlights one of the functional advantages of an adaptive change in the magnitude and sign of interaction – sensitivity to the orthogonal direction remains high despite changes in the response functions. In addition, the dashed curves representing predictions from

independent opponent mechanisms can only predict maximum threshold elevation in one or the other cardinal direction (except for the case where thresholds are elevated equally in all directions). The pattern of results showing maximum elevations in intermediate directions refutes this prediction, and was used by Krauskopf et al. (1986a) as the basis for postulating multiple higher-order color mechanisms. The solid curves show that this pattern of threshold elevations can be predicted by adaptive changes in interaction between just two opponent mechanisms.

An alternative analysis of the thresholds around W in Fig. 7A–D, in terms of discrimination ellipses, provides an intuitive feel for the adaptive change in the combination of the opponent signals. For these thresholds $F_{rg} = F_{yv} = 0$, and the response function can be taken as linear in the neighborhood of zero with a slope equal to $1/\alpha_i$. Equation 3 is simplified so that the response R_i is equal to Q_i/α_i . The analysis can be simplified by replacing the probability summation-based decision rule by a Euclidean response combination rule that sets the threshold in any direction equal to the probe amplitude at which a combined response given by

$$R_{comb}^2 = R_{rg}^2 + R_{yv}^2 = \left(\frac{P_{rg} - \kappa_{yv} P_{yv}}{\alpha_{rg}} \right)^2 + \left(\frac{P_{yv} - \kappa_{rg} P_{rg}}{\alpha_{yv}} \right)^2 \quad (9)$$

reaches some constant criterion value. When the right-hand side of (9) is expanded and set equal to a constant:

$$\left(\frac{1}{\alpha_{rg}^2} + \frac{\kappa_{rg}^2}{\alpha_{yv}^2} \right) P_{rg}^2 + \left(\frac{1}{\alpha_{yv}^2} + \frac{\kappa_{yv}^2}{\alpha_{rg}^2} \right) P_{yv}^2 - 2 \left(\frac{\kappa_{yv}}{\alpha_{rg}^2} + \frac{\kappa_{rg}}{\alpha_{yv}^2} \right) P_{rg} P_{yv} = \text{constant} \quad (10)$$

If the κ_i 's are both zero, then (10) includes nonzero coefficients for the square terms P_{rg}^2 and P_{yv}^2 , but no nonzero coefficients for the cross-product term $P_{rg} P_{yv}$, i.e. it will describe either a circle or an ellipse with major axis aligned along RG or YV . For the pre-adaptation response parameters, the thresholds predicted from (10), plotted on the same axes as Fig. 7, form a circular pattern consistent with the data. If a particular adaptation procedure increases one or both α_i 's but leaves κ_i 's unchanged at zero, the circle will be elongated into an ellipse with major axis along one of the cardinal axes, consistent with the RG and YV adaptation data in Fig. 7A, B. The major axis of the ellipse will tilt towards an intermediate direction if, and only if, there are significant coefficients for the cross-product term in the expression, i.e. if the κ_i 's are not equal to zero. The major axis will fall in the 0° – 90° quadrant if both κ_i 's are positive, and in the 90° – 180° quadrant if both are negative. Therefore, if there are just two discrete classes of opponent mechanisms, then the patterns of post-adaptation results in Fig. 7C, D require changes in mutual interaction between them, irrespective of the decision rule.

12 Shifts in color appearance

Besides discrimination thresholds, the effects of chromatic adaptation have traditionally been studied by matching the appearance of tests in a patch of retina exposed to the adapting stimulus to fields in a patch of retina under neutral adaptation (Wyszecki and Stiles, 1982). Webster and Mollon (1991) showed that there were systematic shifts in color appearance when the adapting stimuli consisted of modulations along color lines. We have used our model to simulate the shifts in color appearance that would be predicted for lights whose chromaticities fall on a circle of radius 6 centered at W in Fig. 2, if they were presented in the test configuration in Fig. 3 after adapting to the modulations used in this study. The α 's, β 's and κ 's for the pre- and post-adaptation conditions were those estimated from the fits to the threshold data for observer K.B. Each light on the circle (spaced at angles of 22.5°), was defined in terms of its projections (rg_N, yv_N). For each post-adaptation condition we calculated the response of the two opponent mechanisms to this light [$R_{rg}^{post}(rg_N), R_{yv}^{post}(yv_N)$], using the post-adaptation parameters. We then assumed that (rg_N, yv_N) imaged on a patch of adapted retina would match a different light (rg_M, yv_M) imaged on a patch of retina under steady adaptation to W , if and only if

$$R_{rg}^{pre}(rg_M) = R_{rg}^{post}(rg_N) \quad (11a)$$

and

$$R_{yv}^{pre}(yv_M) = R_{yv}^{post}(yv_N) \quad (11b)$$

The values for (rg_M, yv_M) were obtained simply by using the following back-transformed version of (2) and (3):

$$rg_M = \frac{1}{1 - \kappa_{yv} \kappa_{rg}} \left[\frac{\alpha_{rg}}{\beta_{rg}} (e^{\beta_{rg} R_{rg}} - 1) + \frac{\kappa_{yv} \alpha_{yv}}{\beta_{yv}} (e^{\beta_{yv} R_{yv}} - 1) \right] \quad (12a)$$

$$yv_M = \frac{1}{1 - \kappa_{yv} \kappa_{rg}} \left[\frac{\alpha_{yv}}{\beta_{yv}} (e^{\beta_{yv} R_{yv}} - 1) + \frac{\kappa_{rg} \alpha_{rg}}{\beta_{rg}} (e^{\beta_{rg} R_{rg}} - 1) \right] \quad (12b)$$

where the α 's, β 's, κ 's are the pre-adaptation parameters for the observer, $R_{rg} = R_{rg}^{post}(rg_N)$ and $R_{yv} = R_{yv}^{post}(yv_N)$. The simulation results are shown in Fig. 8A–D for adaptation to modulation along the RG , YV , 45 – 225° , and 135 – 315° lines respectively. Each panel is centered at W with RG and YV as axes. Under steady adaptation to W , the center appears achromatic, saturation increases along each radial line out from W , and lights along a circle centered at W vary systematically in dominant hue. In each panel the open circles show the chromaticities (rg_N, yv_N) of the test colors, the filled circles show the chromaticities (rg_M, yv_M) of the matched colors, and the dashed line shows the direction of adapting modulation. In each panel, after modulated stimulation, lights on the circle are matched by lights that fall on an ellipse whose

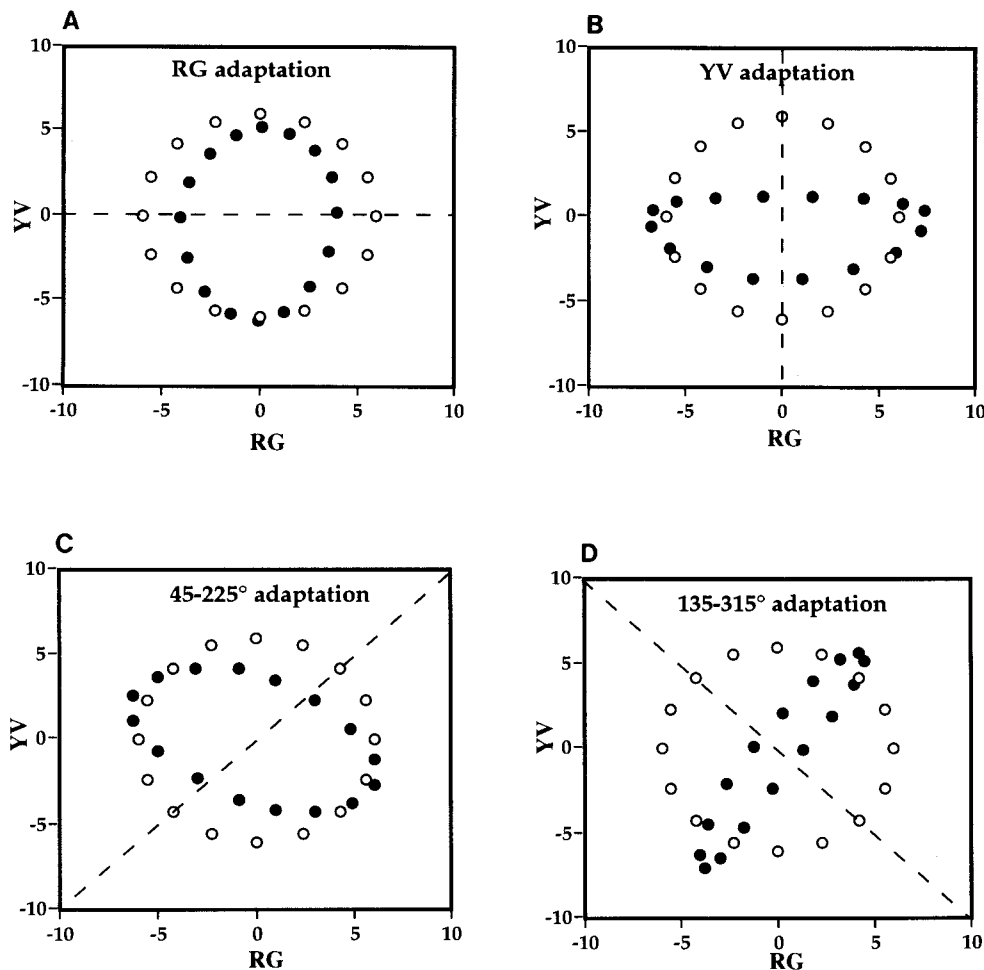


Fig. 8. Numerical simulations of shifts in color appearance after adaptation to modulation along the **A** *RG*, **B** *YV*, **C** $45\text{--}225^\circ$, and **D** $135\text{--}315^\circ$ directions. The *open circles* in all panels represent the chromaticities of test lights imaged on a post-adapted part of the retina. The *filled circles* represent the chromaticities of lights imaged on a pre-adapted part of the retina that will match the test lights in appearance. The parameters used for the simulations were those estimated from Figs. 4 and 7

major axis is roughly orthogonal to the adapting direction. The simulations predict two main effects on appearance: a decrease in perceived saturation of lights that fall on or near the adaptation locus, and a shift in perceived hues away from the adaptation locus. These shifts are qualitatively similar to those measured by Webster and Mollon (1991). It is worth reiterating that without a change in interaction parameters, it is not possible to get ellipses oriented along other than the cardinal directions. Any difference between simulated results and empirical measurements in the size of the ellipses is probably not important. We find that we can shrink the size of our ellipses by assuming a greater amount of adaptation. Krauskopf and Zaidi (1985, 1986) found that the effect of adapting to modulated colors is greater when the modulated and test fields are spatially identical, as was the case in Webster and Mollon's procedure. There is one major point of disagreement. Webster and Mollon (1991) reported decreases in perceived saturation along each cardinal axis after adaptation to modulation along the orthogonal axis. The simulations predict no such change, which corresponds to the absence of significant threshold elevations after adaptation to orthogonal modulation. The causes of this difference between thresholds and asymmetrical matches are not clear.

13 Adaptive orthogonalization

The purpose of adaptive processes at early stages of the visual system is to provide an efficient representation of signals for succeeding stages. At every stage, stimuli that vary on more than one dimension are represented by the distribution of responses of different classes of elements with limited dynamic range, each class predominantly sensitive to one of the dimensions. Discrimination is based on the difference in combined response, i.e. "distance" in a multidimensional representation space. If a majority of the target stimuli are represented in a restricted angular area of this space, discrimination performance can be improved on average by introducing a mutual interaction between different classes so as to expand the angular extent of this area, thus increasing the "distance" between the representations of the relevant stimuli (Barlow 1990). In general, the optimal representation corresponds to a level of interaction at which the responses of different classes to the target stimuli are mutually orthogonal on average (Kohonen 1984). We show below that the magnitude of interaction between opponent mechanisms in different states of adaptation is consistent with an adaptive orthogonalization process.

In our functional model, the values of κ_i 's are dynamically adjusted in proportion to the correlation or the scalar product of the stimulations $Q_{rg}(t)$ and $Q_{yv}(t)$ during the adaptation interval:

$$\frac{d(\kappa_{rg}, \kappa_{yv})}{dt} = -\delta \int_A Q_{rg}(t) Q_{yv}(t) dt \quad (13)$$

where δ is a constant governing the rate of change and A is the adaptation interval. The stable state is reached when $d\kappa/dt = 0$, i.e. when $Q_{rg}(t)$ is orthogonal to $Q_{yv}(t)$. This idea adapted is from Kohonen and Oja (1976) and Barlow and Foldiak (1989). Substituting from (2), the stable state is reached for the values of κ_{rg} and κ_{yv} that satisfy:

$$\int_A [rg(t) - \kappa_{yv} yv(t)] [yv(t) - \kappa_{rg} rg(t)] dt = 0 \quad (14)$$

The adapting stimuli in this study consisted of sinusoidal temporal modulation of chromaticities along a color line of angle ϑ . Therefore, during adaptation $rg(t) = \cos(\vartheta) \sin(t)$ and $yv(t) = \sin(\vartheta) \sin(t)$, and (14) simplifies to:

$$(\cos \vartheta - \kappa_{yv} \sin \vartheta)(\sin \vartheta - \kappa_{rg} \cos \vartheta) = 0 \quad (15)$$

Since this is only one equation in two unknowns, κ_{rg} , and κ_{yv} , there is no unique solution. However, it is obvious that if the angle of adapting modulation ϑ is equal to 0° or 90° , the conditions for a stable state are satisfied when $\kappa_{rg} = \kappa_{yv} = 0$, consistent with the empirical results. For intermediate values of ϑ the stable state conditions are satisfied by:

$$\kappa_{rg} = \frac{\sin \vartheta}{\cos \vartheta} \quad (16a)$$

$$\kappa_{yv} = \frac{\cos \vartheta}{\sin \vartheta} \quad (16b)$$

For $\vartheta = 45^\circ$, the stable values are $\kappa_{rg} = \kappa_{yv} = 1$ and for $\vartheta = 135^\circ$, $\kappa_{rg} = \kappa_{yv} = -1$. The κ_i 's required for the fits in Fig. 7 had the predicted signs but smaller magnitudes. This may partially be because the adaptation process progresses towards but does not reach a stable state in our experimental conditions.

In mechanistic terms, adaptive orthogonalization could be achieved by an inter-unit mechanism that computes the scalar product of the two time-varying functions $Q_{rg}(t)$ and $Q_{yv}(t)$ and modifies the values of κ_i 's at the input to Q_j 's according to (13). However, the simplicity of the stable-state solutions in (16a, b) shows that adaptive orthogonalization will also result if at each Q_i node the value of κ_j is adaptively set to minimize $\int_A Q_i(t) dt$. At ϑ equal to 0° or 90° , $\kappa_{rg} = \kappa_{yv} = 0$ leads to the minimization of the two signals. For intermediate values of ϑ , the minimization rule is equivalent to setting κ 's so that:

$$\int rg(t) dt - \kappa_{yv} \int yv(t) dt = 0 \quad (17a)$$

$$\int yv(t) dt - \kappa_{rg} \int rg(t) dt = 0 \quad (17b)$$

The solutions for (17a, b) are identical to the orthogonal-state values of κ_i 's in (16a, b). The minimization rule has the advantage that a process that sets the efficacy of a synapse based on the time-integrated difference between the values of two signals will be easier to implement than one that depends on taking the scalar product of two time-varying functions. In addition, in this scheme adaptive orthogonalization can be achieved by using a feed-forward process instead of the feed-back networks proposed by Kohonen and Oja (1976), Barlow and Foldiak (1989), and Atick et al. (1993).

Changing κ 's from zero to positive values as a result of prolonged modulation along the 45 – 225° line transforms the space so that the angular area around the 45 – 225° line expands and the area around the orthogonal 135 – 315° line shrinks. As a result, discrimination is improved in the direction orthogonal to the adapting modulation (Fig. 7C). This distortion of the representation space is also reflected in the orientation of the major axis of the ellipse in Fig. 8C – hues in the vicinity of the 45 – 225° line appear more dissimilar after adapting to modulation along this line than under steady adaptation to W , and hues in the vicinity of 135 – 315° appear more similar.

Psychophysical results that are inconsistent with independent opponent mechanisms, can be explained either by adaptive orthogonalization or the higher-order color mechanisms of Krauskopf et al. (1986a, b). Since a model with multiple higher-order mechanisms will have a larger number of parameters, adaptive orthogonalization has the virtue of parsimony. Could physiological measurements critically decide between these theories? The studies by Derrington et al. (1984) and Lennie et al. (1990) are the most relevant because they used stimuli similar to the adapting modulations in this study. Derrington et al. (1990) found that neurons in macaque parvo-LGN clustered in two classes with respect to their chromatic properties. These classes corresponded to the opponent mechanisms in our model. In macaque cortical area V1, Lennie et al. (1990) found that though the responses of neurons were proportional to linear combinations of cone signals, those showing color opponency did not fall into the two groups seen in the LGN. Some neurons showed unusually sharp chromatic selectivity. Since the responses of cortical neurons can be described as linear combinations of responses (possibly rectified) of the two classes of LGN neurons, the question reduces to whether the combination rule for each neuron is hard-wired or adaptable. This experiment remains to be performed.

14 Adaptive response nonlinearities

Since visual mechanisms have limited dynamic range, their sensitivity has to be modifiable in order for an organism to function in a large variety of naturally occurring light environments. The differences between the filled and open symbols in Fig. 4A, B indicate that differential sensitivity over the dynamic range is governed not just by the mean adaptation level but also by the

distribution of inputs present in the adapting stimulus. As shown earlier, this difference cannot be explained by multiplicative "fatigue" (also see Shapiro and Zaidi 1992b). We present a theory below that postulates that the most efficient use of a limited response range is to match the shape of the response function to the distribution of inputs, so that on average each level of response is equally probable. This theory explains why threshold curves are flatter after adaptation to sinusoidal modulation than during adaptation to a steady uniform field of the same average color.

In any state of steady adaptation to a uniform field, the range of lights an observer can discriminate is severely limited. An observer can detect fairly small differences between lights that are similar to the adapting background, but requires fairly large differences to discriminate between lights that are further from the adapting background. Craik (1938) showed that for a large range of steady brightness levels, brightness discrimination threshold curves shift with the adapting level so that the minimum is at or near the steady adapting brightness level. Chromatic discrimination along the cardinal axes shows similar tendencies. The V-shaped curve formed by the open circles in Fig. 4A shows that thresholds for *RG* discrimination are minimum at *W* under steady adaptation to *W*. Shapiro and Zaidi (1992b) showed that when steady adaptation is shifted to other points on the *RG* axis, the V-shaped curve shifts laterally so that the magnitude of the minimum threshold stays constant but the locus of the minima coincides with the adaptation point. The *YV* discrimination threshold curve also shifts mainly laterally so that the minimum coincides with the adaptation point on the *YV* axis; there are also small vertical shifts in the curve so that the minimum threshold is a monotonically increasing function of the level of *S*-cone excitation by the adapting light. Craik (1938) conjectured that this adaptation could be due to gain changes in mechanisms with a limited response range. Barlow (1969) and others have shown that the contrast response of ganglion cells at different adaptation levels is in accord with this conjecture. Zaidi et al. (1992) showed that the shifts in threshold curves along the *YV* axis is consistent with independent multiplicative gain changes in the *S* and *L + M* paths. In general the shift in response range due to multiplicative gain changes as a function of adapting level provides an adequate explanation for adaptation to backgrounds that are uniform in time and space.

The present procedure consisted of adaptation to a background whose color varied in time. Similarly, adaptation to drifting spatial sinusoids (Greenlee and Heitger 1988) is adaptation to a background whose color varies in both space and time. The results in Figs. 4A, B and in Greenlee and Heitger (1988) require a change in shape of the response function. The theory we propose in this section requires that the response function of each mechanism be adjusted not just by the mean level of the adapting background, but by the distribution of excitation levels in the adapting stimulus.

We will assume without loss of generality, that on the positive side of the adaptation point, for each mechanism $0 \leq Q \leq 1$, $0 \leq R \leq 1$, and the probabilities of occur-

rence of different levels of input and response are $\Phi_Q(q) = \text{Prob}(Q = q)$, $\Phi_R(r) = \text{Prob}(R = r)$. We constrain the response, $R = f(Q)$, to be a continuous and monotonically increasing function of Q , so that $r = f(q)$ and $q = f^{-1}(r)$. If the differential response of the mechanism at each input level is set equal to the relative frequency of that input level in the adapting stimulus:

$$\frac{dR}{dQ_{Q=q}} = \Phi_Q(q) \quad (18)$$

Then:

$$r = \int_0^q \Phi_Q(y) dy \quad (19)$$

$\Phi_Q(q)$ versus q is the histogram of the distribution of input values. R is therefore set equal at each input level to the cumulative probability distribution of Q . This implies that $\Phi_R(r) = 1$ for all $0 \leq r \leq 1$, because

$$\begin{aligned} \int_0^r \Phi_R(x) dx &= \text{Prob}(R \leq r) = \text{Prob}[f(Q) \leq r] \\ &= \text{Prob}[Q \leq f^{-1}(r) = q] \\ &= \int_0^q \Phi_Q(y) dy = r \end{aligned} \quad (20)$$

As a result of this process, each response level is equally probable, i.e. the entire dynamic range of the mechanism is used most efficiently. A symmetric analysis would be performed on the negative side of the adaptation point. Since the histogram of input values to the three cardinal mechanisms provides a global description of a stimulus, this process enhances the effective contrast in an adapting stimulus, similar to the histogram modification techniques used in digital image enhancement (Rosenfeld and Kak 1982; Gonzalez and Wintz 1987). Swain and Ballard (1991) describe other useful aspects of three-dimensional color histograms.

We now derive the implications of response equalization for a mechanism adapted first to temporal modulation of its inputs, and second to a steady average level. For a triangular wave of unit contrast, $\Phi_Q(q) = \text{constant} = 1/\alpha$. Therefore, by this theory, after adaptation to triangular modulation is complete, $R = Q/\alpha$. Because R is a linear function of Q , the predicted probe thresholds will all equal α , i.e. the threshold curve will have zero slope with an intercept equal to α . For a sinusoidal modulation, $\Phi_Q(q)$ has a bowed shape with a minimum at *W*. Therefore, in the post-adaptation condition, the threshold curves should slope downwards from *W*. In general, we find the post-adaptation curves, as in Fig. 4A, B, have shallower slopes than the pre-adaptation curves, but are not even completely flat. There is one example of a downward slope in Shapiro and Zaidi (1992b), and Greenlee and Heitger (1988) found flat post-adaptation contrast discrimination curves when stimuli were restricted in spatial frequency. The changes in the slopes are therefore in the direction predicted by theory, but the magnitude of the change is less than the predicted. Whether this is due to less than complete adaptation

needs to be tested. For a steady uniform field at W , $\Phi_Q(q) = 1$ for $q = 0$, and $\Phi_Q(q) = 0$ elsewhere. This theory predicts that R should be a step function of Q at zero, and that there should be perfect discriminability of any transition from $Q = 0$, but no discriminability at any other input level. This state of affairs is obviously never reached. It is unreasonable to expect a maximum response to the smallest perturbation from the dc level, and there is probably a limit to how much α can be decreased and β increased in the function in (3). It may also be possible that the most efficient use of the dynamic range is not a uniform probability distribution of response levels, but rather $\Phi_R(r) = g(r)$, where g is some smooth function that weights factors like reliability and metabolic cost. In this case the optimal response function will be $R = g^{-1}[f(Q)]$ where $f(Q)$ is the cumulative distribution. This theory is tentative, because although it is consistent with some observations, it has not yet been tested critically. With presently existing data it is not clear whether the effective aspect of the adapting stimulus is the shape of the histogram or just the range of input values.

There are two complexities in relating the response equalization process to physiological measurements. First, the responses of cortical neurons have been measured after prolonged luminance modulation (e.g. Movshon and Lennie 1979; Sclar et al. 1989), but not after prolonged chromatic modulation. Second, it is not clear whether the psychophysically inferred response linearization is related to the response of single neurons or to the combined response of an aggregate of neurons. In macaque V1 neurons, adaptation to high-luminance-contrast sinusoidal gratings of optimal spatial frequency and orientation changes the parameters of the contrast-response function, so that detectability of low-contrast gratings is reduced but the discriminability of high-contrast stimuli is improved by extending the operating range (Sclar et al. 1989). Therefore, even in individual neurons the response curve is shaped to some extent by the history of stimulation. Laughlin (1981) has provided evidence that the input-output function of inter-neurons in the fly's eye is matched to the expected distribution of contrasts in natural scenes.

15 Adaptation, memory and learning

In visual perception, stored knowledge about naturally occurring distributions and associations is essential in making veridical inferences (von Helmholtz 1925). Barlow (1990) has pointed out that learning and adaptation both involve acquisition, storage, and use of background knowledge of the sensory environment. This paper provides evidence for adaptation to associations and distributions of input values. Since information about these qualities is contained in the parameters of the model, it is tempting to think that associative memory may be built upon successive adaptations of these types. However, a number of considerations suggest caution. The functional models discussed in this paper optimize the efficient representation of signals for the next stage of

processing, and are not concerned with learning a specific set of inputs. Learning facilitates the choice of the appropriate response from among multiple stored responses, whereas adaptation matches sensitivity to stimulation within a limited interval and is useful only to the extent that the present distribution of lights is similar to the preceding history. Moreover, even though adaptation to complex attributes is slower than dc adaptation, the time courses of acquisition and decay are fairly similar – decay is simply adaptation to a new stimulus. For useful stored knowledge, the rate of decay should hopefully be much slower than the rate of acquisition. On this basis, the kind of long-lasting adaptation involved in the McCollough (1965) effect may be more similar to the process involved in learning (Barlow and Foldiak 1989).

16 Discussion

The results of this study are relevant to two issues: (i) human color vision mechanisms subsequent to the opponent combination of cone signals, and (ii) visual adaptation to modulated stimuli. When the two opponent-color mechanisms are simultaneously stimulated for a prolonged period, chromatic discrimination and appearance are affected in a manner that depends on the magnitude and sign of the correlation. Simulations show that these effects can be explained by a simple modification to traditional color theory, i.e. by allowing an adaptable linear interaction between the two opponent mechanisms. The magnitude and sign of interaction change in a manner that is consistent with an adaptive orthogonalization process. It remains to be seen whether this simple form of interaction is sufficient to explain the effects of correlated stimulation that is not confined to a single color line. In addition, prolonged stimulation modifies the response of each opponent mechanism as an adaptive function of the distribution of inputs, rather than of just the mean input level. In the response equalization process proposed here, the shape of each response function is set by matching differential sensitivity to the relative frequency of input levels. This process is optimal, but unrealistic in that it requires the visual system to extract the complete frequency distribution of input levels. It remains to be tested whether the results can be explained in terms of adaptation to a discrete set of low-order moments of the adapting distribution.

Acknowledgements. We thank John Krauskopf and Ben Sachtler for discussions, Nina Zipser for checking derivations, Su-Jean Hwang for manuscript preparation, and Karen Burhans for patient observation. This research was supported by National Eye Institute through grant EY07556 to Q. Zaidi.

References

- Atick JJ, Li Z, Redlick AN (1993) What does post-adaptation color appearance reveal about cortical color representation? *Vision Res* 33:123–130
- Barlow HB (1969) Pattern recognition and the responses of sensory neurones. *Ann NY Acad Sci* 156:872–881

- Barlow HB (1990) A theory about the functional role and synaptic mechanism of visual after-effects. In: Blakemore C (ed) *Vision: encoding and efficiency*. Cambridge University Press, pp 363–375
- Barlow HB, Foldiak PF (1989) Adaptation and decorrelation in the cortex. In: Durbin RM, Miall C, Mitchison GJ (eds) *The computing neuron*. Addison-Wesley, New York, pp 54–72
- Boynton RM, Nagy AL, Eskew RT Jr (1986) Similarity of normalized discrimination ellipses in the constant-luminance chromaticity plane. *Perception* 15:755–763
- Craik KJW (1938) The effect of adaptation on differential brightness discrimination. *J Physiol* 92:406–421
- Derrington AM, Krauskopf J, Lennie P (1984) Chromatic mechanisms in lateral geniculate nucleus of macaque. *J Physiol* 357:241–265
- Flanagan P, Cavanagh P, Favreau DE (1990) Independent orientation-selective mechanisms for the cardinal directions of color space. *Vision Res* 30:769–778
- Gegenfurtner K, Kiper D (1992) Contrast detection in chromatic and luminance noise. *J Opt Soc Am [A]* 9:1880–1888
- Gonzalez RC, Wintz P (1987) *Digital image processing*. Addison-Wesley, Reading, Mass
- Greenlee MW, Heitger F (1988) The functional role of contrast adaptation. *Vision Res* 28:791–797
- Helmholtz H von (1925) *Physiological optics*, vol. 3. Optical Society of America, Washington
- Judd DB (1932) Chromaticity sensibility to stimulus differences. *J Opt Soc Am* 22:72–108
- Kohonen T (1984) *Self-organization and associative memory*. Springer, Berlin Heidelberg New York
- Kohonen T, Oja E (1976) Fast adaptive formation of orthogonalizing filters and associative memory in recurrent networks of neuron-like elements. *Biol Cybern* 21:85–95
- Krauskopf J, Zaidi Q (1985) Spatial factors in desensitization along cardinal directions of color space. *Invest Ophthalmol Vis Sci* 26:206
- Krauskopf J, Zaidi Q (1986) Induced desensitization. *Vision Res* 26:759–762
- Krauskopf J, Williams DR, Heeley D (1982) Cardinal directions of color space. *Vision Res* 22:1123–1131
- Krauskopf J, Williams DR, Mandler MB, Brown AM (1986a) Higher order color mechanisms. *Vision Res* 26:23–32
- Krauskopf J, Zaidi Q, Mandler MB (1986b) Mechanisms of simultaneous color induction. *J Opt Soc Am [A]* 3:1752–1757
- Laughlin S (1981) A simple coding procedure enhances a neuron's information capacity. *Z Naturforsch* 36:910–912
- Le Grand Y (1949) Le seuils différentiels de couleurs dans la théorie de Young. *Rev Opt Theo Inst* 28:261–278
- Lennie P, Krauskopf J, Sclar G (1990) Chromatic mechanisms in striate cortex of macaque. *J Neurosci* 10:649–669
- MacLeod DIA, Boynton RM (1979) Chromaticity diagram showing cone excitation by stimuli of equal luminance. *J Opt Soc Am [A]* 69:1183–1186
- McCollough C (1965) Color adaptation of edge-detectors in the human visual system. *Science* 149:1115–1116
- Movshon JA, Lennie P (1979) Pattern-selective adaptation in visual cortical neurones. *Nature* 278:850–852
- Press W, Flannery B, Teukolsky S, Vetterling W (1988) *Numerical recipes in C: the art of scientific computing*. Cambridge University Press, New York
- Rosenfeld A, Kak AC (1982) *Digital picture processing*. Academic Press, New York
- Sachtler W, Zaidi Q (1992) Chromatic and luminance signals in visual memory. *J Opt Soc Am [A]* 9:877–894
- Sclar G, Lennie P, DePriest DD (1989) Contrast adaptation in striate cortex of macaque. *Vision Res* 29:747–755
- Shapiro AG, Zaidi Q (1992a) Prolonged temporal modulation and the interaction between color mechanisms. *Opt Soc Am Tech Digest Ser* 23–51
- Shapiro AG, Zaidi Q (1992b) The effect of prolonged temporal modulation on the differential response of color mechanisms. *Vision Res* 32:2065–2075
- Smith VC, Pokorny J (1975) Spectral sensitivity of the foveal cone photopigments between 400 and 700 nm. *Vision Res* 15:161–171
- Swain MJ, Ballard DH (1991) Color indexing. *Int J Comput Vision* 7:11–32
- Webster MA, Mollon JD (1991) Changes in colour appearance following post-receptoral adaptation. *Nature* 349:235–238
- Wyszecki G, Stiles WS (1982) *Color science*, 2nd Edn. Wiley, New York
- Zaidi Q (1992) Parallel and serial connections between human color mechanisms. In: Brannan JR (ed) *Applications of parallel processing in vision*. Elsevier, New York, pp 227–259
- Zaidi Q, Halevy D (1991) Chromatic mechanisms beyond linear opponency. In: Valberg A, Lee BB (eds) *Pigments to perception*. Plenum Press, New York, pp 337–348
- Zaidi Q, Halevy D (1993) Visual mechanisms that signal the direction of color changes. *Vision Res* 33:1037–1051
- Zaidi Q, Shapiro A (1992a) Combination of signals from opponent color mechanisms. *OSA Adv Color Vision Tech Digest* 4:201–203
- Zaidi Q, Shapiro A (1992b) Adaptive decorrelation between opponent-color mechanisms. *Perception* 21 [Suppl 2]:62
- Zaidi Q, Shapiro A, Hood DC (1992) The effect of adaptation on the differential sensitivity of the S-cone color system. *Vision Res* 32:1297–1318